Transportation Research Interdisciplinary Perspectives 21 (2023) 100866

Contents lists available at ScienceDirect

Transportation Research Interdisciplinary Perspectives

journal homepage: www.elsevier.com/locate/trip

Double-layer control architecture for motion and torque optimisation of autonomous electric vehicles

Angelo Coppola [a], Gianmaria De Tommasi [b], Carlo Motta [b,*], Alberto Petrillo [b], Stefania Santini [b]

[a] Department of Civil, Architectural and Environmental Engineering, University of Naples "Federico II", Naples, Italy
[b] Department of Electrical Engineering and Information Technology, University of Naples "Federico II", Naples, Italy

ARTICLE INFO

Keywords:
Sustainable mobility
Electric vehicle
Energy saving control architecture
Energy consumption optimisation
Virtual testing

ABSTRACT

Optimising energy autonomy for autonomous electric vehicles is a significant challenge in sustainable and environmentally friendly mobility. To this end, we propose a novel double-layer control architecture designed to drive the longitudinal motion of electric vehicles equipped with a regenerative braking system. The first layer resembles an Adaptive Cruise Control, while the second one is enabled during the braking phase and is devoted to the blending between the motor torque and the hydraulic one. This layer is synthesised as a Nonlinear Model Predictive Control strategy so as to maximise the efficiency of the regenerative system. The control architecture, by combining the two control strategies, allows to reduce the overall energy consumption for electric vehicles, while simultaneously ensuring a safer, more sustainable, and comfortable driving experience. Additionally, this combination is capable of compensating for any efficiency issues arising from external factors, such as different traffic conditions encountered by the vehicle. To evaluate the effectiveness of the proposed control architecture, extensive simulation analysis was carried out using the MiTraS virtual testing platform, considering two realistic driving scenarios. Results confirm the robustness and safety of the proposed control architecture in ensuring the tracking of the desired trajectory while optimising the energy consumption.

1. Introduction

Electric Vehicles (EVs) are considered the most promising and viable near-term technology to reduce the exploitation of fossil fuels and resulting greenhouse gas emissions produced by conventional vehicles (Valentina et al., 2019). Although sustainability and environmental benefits have a major influence on the EVs' adoption, they are usually behind performance in the customers' ranking (Egbue and Long, 2012; Chhikara et al., 2021); it follows that the maximisation of EVs' range autonomy is one of the main aspects for their massive market deployment (Sun et al., 2021) (the interested reader could refer to Maybury et al. (2022), Wu and Kontou (2022) for a more detailed discussion about factors and incentives for the adoption of electric vehicles).

An effective way to counteract this drawback is to exploit regenerative braking systems (RBS) enabling the energy transformation from kinetic to electric so to recharge the electric battery. Indeed, it has been shown that this technology is able to increase EV's autonomy of about 15% (Nian et al., 2014), and larger values can be obtained in traffic-congested areas where both *stop&go* and *slow&go* phenomena are very frequent (Kumar and Subramanian, 2016; Zhang et al., 2017). This motivates the great interest during recent years, from both industry and academia, in designing these systems (Ko et al., 2014b; Lv et al., 2015). A great research effort has been put in controlling a fully electric regenerative braking system (FE-RBS), where the total braking torque is provided by the electric motor (Xu et al., 2015; Liu et al., 2021). However, since this latter works only within certain operative ranges, the vehicle may need a relatively long time to complete a braking manoeuvre and this results in a reduction of safety (Tao et al., 2017). Thus, the torque provided by the hydraulic braking, typically larger than the electric one, is usually needed in order to provide adequate and safe braking deceleration (Zhao et al., 2018). A breakthrough vehicle configuration allowing to overcome the limitations of FE-RBS is the four-motorised-wheel EV (4MWEV), which employs four in-wheel motors (Nam et al., 2012). In this latter configuration, the drive/regenerative brake torque for each wheel is controlled separately; hence it is possible to enhance the overall vehicle efficiency through the torque distribution among in-wheel electric motors, as well as through the coordination between hydraulic braking torque and motor braking one (Gang and Zhi, 2018; Chen et al., 2019). Leveraging the 4MWEV configuration, several different energy-saving and efficient control strategies have been proposed in the technical literature to deal

* Corresponding author.
E-mail addresses: angelo.coppola@unina.it (A. Coppola), gianmaria.detommasi@unina.it (G. De Tommasi), carlo.motta@unina.it (C. Motta), alberto.petrillo@unina.it (A. Petrillo), stefania.santini@unina.it (S. Santini).

https://doi.org/10.1016/j.trip.2023.100866
Received 20 August 2022; Received in revised form 1 May 2023; Accepted 19 June 2023
Available online 28 June 2023

with the following two critical issues: (*i*) how to coordinate hydraulic braking and regenerative braking under the premise of braking safety; (*ii*) how to distribute the braking torque between the front and rear wheels so as to obtain the maximum braking strength. To solve the aforementioned problems, heuristic approaches- e.g. rules-based (Ko et al., 2014b) or fuzzy logic (Xin et al., 2019)- have been widely suggested in the technical literature. Nevertheless, these approaches are strongly dependent on simulation experiments carried out to define fuzzy and/or rules sets, and may lead to lower control accuracy as well (Petrillo et al., 2023). To improve the energy-recovery efficiency, more advanced control techniques are proposed, such as optimal control (Kanarachos et al., 2014), Model Predictive Control (MPC) (Guo et al., 2019) or Nonlinear MPC (NMPC) (Li et al., 2018)

However, it is worth highlighting that the range of electric vehicles is strongly influenced not only by the design of the braking torque distribution but also by the driving style (Mruzek et al., 2017; Araque et al., 2018). Indeed, experimental results have proved a 6%–10% fuel economy improvement when unnecessary acceleration and deceleration manoeuvres are minimised (Lee et al., 2021; Bifulco et al., 2021). To this end, Autonomous Electric Vehicles (AEVs) have received a lot of attention due to their ability to optimally plan and execute driving operations through the usage of the surrounding road traffic environment information as obtained from detection technologies (Coppola et al., 2022). Based on the above facts, it is possible to appreciate how the proper combination of Advanced Driving Assistance System (ADAS) functionalities with local torque optimisation features can enhance the battery range of EVs. Within this framework, this paper deals with the problem of designing a novel energy-oriented control architecture for AEVs able to achieve a twofold objective, namely: (*i*) a proper planning/execution of the manoeuvres to be imposed to AEVs which avoids strong acceleration/deceleration manoeuvres while guaranteeing driving safety; (*ii*) the proper coordination/distribution of the EV braking torque for optimal energy recovery. To this aim, we propose a novel hierarchical double-layer integrated control architecture able to simultaneously accomplish the aforementioned task with two layers, where the first one is devoted to the computation of longitudinal motion of the vehicle in order to avoid strong acceleration/deceleration manoeuvres while the second one is devoted to the optimisation of the energy recovery during braking phases. This implies an improvement of the sustainability level for AEVs (Kovačić et al., 2022; Onat and Kucukvar, 2022). More specifically, the first layer, designed for imposing a behaviour that resembles an Adaptive Cruise Control (ACC), computes the required traction/braking torque control signal (i.e. the input of the controlled object) to achieve safe and smooth trajectory tracking goals. A PID-like controller drives the longitudinal motion of the autonomous EVs for maintaining a safe distance w.r.t. a predecessor vehicle ahead, hence avoiding strong acceleration/deceleration manoeuvres and ensuring energy-saving consumption. The second layer enabled only when performing braking manoeuvres aims at optimising the torque distribution between motor and hydraulic braking, as well as between the front and rear parts of the vehicle. This layer, synthesised according to an NMPC approach, is purposely designed to guarantee a safe braking performance while maximising the efficiency of the regenerative system.

More notably, an extensive performances evaluation analysis, carried out by leveraging the virtual testing simulation platform MiTraS (Caiazzo et al., 2021), confirms the theoretical results in realistic driving scenarios and allows evaluating the robustness of the approach w.r.t. unmodelled vehicle dynamics and unavoidable parameters uncertainties. Indeed, the simulations campaign is carried out also considering vehicle uncertainties emulated via the Latin Hypercube Sampling (LHS) approach, therefore allowing a generalisation of the method and leaving its usage for possible future re-adaptations. It is worth noting that, virtual simulation is a critical and, undoubtedly, fundamental step for the development of autonomous driving technologies. Apart from the major advantage of allowing a safe verification of specific requirements, also in conditions characterised by very broad uncertainty without the risk of real accidents and crashes, its support is crucial to perform comprehensive and cost-effective performance assessments in complex conditions of realistic traffic scenarios which are otherwise prohibitive for conventional small-scale physical testing, whose variability is usually limited by infrastructural and environmental conditions. Therefore, extensive simulation results related to the New European Driving Cycle (NEDC) and involving several tracking performances and energy-saving Key Performance Indexes (KPIs) have been carried out. These results disclose the benefits of the proposed control architecture in guaranteeing the tracking of a desired smooth motion profile while increasing the energy autonomy of the autonomous EV. These latter aspects have been also highlighted via a comparison analysis w.r.t. other control strategies such as typical PI, rule-based control, and a nonlinear MPC.

Finally, the paper is organised as follows. Section 2 presents the closely related works. Section 3 introduces the control-oriented vehicle dynamical model. The problem statement and the proposed double-layer control architecture are presented in Section 4. Section 5 discusses the validation scenario and the KPIs exploited for the evaluation of the benefits the control architecture could bring to AEVs in terms of energy saving while Section 6 discloses the extensive simulation campaign. Conclusions are drawn in Section 7.

2. Related works

As stated in the introduction, the drive/regenerative brake torque of each wheel of a 4MWEV can be controlled separately through torque distribution among in-wheel electric motors, ensuring more control flexibility with several different purposes of vehicle performance enhancement. Optimal wheel torque distribution for energy efficiency has been deeply examined in a bunch of literature in the past years.

Early attempts exploit rule-based approaches, where a set of rules is employed to determine the percentage of regenerative torque to be applied as a function of the current state of some kinetic variables and road features (Zhang et al., 2013; Ko et al., 2014a; Zhang et al., 2012). For instance, Ko et al. (2014b) proposed a rule-based regenerative control algorithm that computes the proper torque to be imposed on the vehicle by taking into account the driver's braking characteristics, regenerative braking energy, and driving comfort. To evaluate the performance of the proposed brake system regenerative braking cooperative control algorithm, MATLAB/Simulink and CarSim models were employed to carry out a simulation test at the deceleration of 0.2 g from 100 [km/h]. However, this type of strategy lacks flexibility when multiple system constraints are considered, while the presence of various rules with different goals may lead to counterproductive outcomes. Consequently, to better deal with vehicle uncertainty and non-linearity, some researchers leveraged fuzzy control techniques (Maia et al., 2015; Xiao et al., 2017; Xin et al., 2019). Maia et al. (2015) developed a fuzzy model requiring the vehicle's acceleration and jerk and road slope as input variables while returning the ratio of regenerative braking force to the total braking force as output. The performances of the method (battery SOC, total energy required, and energy used in braking) were evaluated considering two simulation scenarios, namely one urban and one extra-urban with 103 [km], and 112 [km] length. Finally, they were compared to the 100% regeneration case, i.e., when all the braking force/energy is converted to electric current and returned to charge the battery. Instead, Xin et al. (2019) dealt with the problem of coordinating the torque distribution between the hydraulic brake and the motor brake systems by developing a fuzzy controller which uses battery State of Charge (SOC) and braking strength as input variables. The simulation analysis carried out in the AVL CRUISE-Simulink co-simulation environment, proved that the driving range of the vehicle with the proposed control strategy increased by 7.74% and the energy recovery rate by 11.05% compare to a rule-based strategy. Along this line, Kanarachos et al. (2014) suggested a braking torque distribution

control scheme based on the state-dependent Riccati equation, the vehicle state estimation, and the magic formula tire model to handle the tire saturation and motor constraints. The simulation analysis, carried out in a MATLAB/Simulink environment and employing different braking scenarios (different values of the friction coefficient), proved the advantages of the proposed controller in terms of recuperated energy w.r.t. a constrained linear quadratic regulator. Again, to improve the model estimation accuracy and the robustness of the control system, Lv et al. (2014) proposed a blended braking control algorithm leveraging an extended Kalman filter for vehicle state estimation that considers damping and elastic properties of the electrified powertrain system. To deal with multiple objectives and constraints for the optimal torque generation and distribution problem while avoiding too high computational effort, Model Predictive Control (MPC) methodology was widely exploited (Wang et al., 2015; Li et al., 2016; Wang et al., 2018; Guo et al., 2019). Within this control framework, Huang and Wang (2012) proposed a Nonlinear MPC (NMPC) aiming at improving the energy recovery via the computation of an optimal distribution between the front and rear braking torques; safety was also ensured by considering hard constraints on the longitudinal slip ratios of the wheels so to avoid locks during deceleration. For the simulation analysis, CarSim and MATLAB/Simulink were employed to model the full vehicle and the control strategy. Two reference speed profiles, each ten seconds long, were designed to cover large ranges of velocities and decelerations. Results showed that the proposed controller was able to encompass a conventional proportional-integral controller and an NMPC with no consideration of the energy recovery in terms of both energy saving and vehicle-speed-tracking performance. However, the torque blending between electric motor braking and hydraulic braking was not taken into account, hence limiting the energy-saving ability of the controller. Basrah et al. (2017) developed both a linear and a nonlinear MPC to achieve optimal blending while simultaneously controlling the front/rear braking distribution. However, the proposed method allows a number of approximations thus making the strategy hard to adapt to a realistic scenario. On top of that, the approach shows some limits due to its formulation (i.e. loss of performance in slip tracking as the vehicle speed approaches zero) which makes the control not-reusable. Conversely, Li et al. (2018) developed a braking strategy based on the driver's braking intention. If the change rate of the brake pedal is lower than a threshold, an NMPC control manages the blending, otherwise, it is considered emergency braking, and a sliding mode control takes over. By changing the weight of the MPC cost function, several braking intentions were modelled. Virtual validation, based on simplified speed profiles lasting between 5 and 10 s, showed the ability of the proposed braking strategy to recycle more energy than a conventional one. However, low regeneration efficiency is a fatal flaw of this strategy. With the aim to deal with multiple objectives and constraints of the regenerative braking system, Xu et al. (2019) proposed a holistic MPC-based braking torque optimisation controller. Specifically, the torque distribution controller maximises the regeneration efficiency by determining the optimal split between hydraulic and motor braking torque, while ensuring brake safety. Nevertheless, no comprehensive analysis confirms the achievement of energy efficiency and braking performance in different realistic uncertain traffic scenarios. The proposed approach is demonstrated via a co-simulation platform, composed of AMESim and Simulink, under simplified driving conditions, i.e., simplified braking speed profiles with different adhesion coefficients. The outcome proved that the regeneration efficiency and braking performance were improved than a rule-based strategy used as the baseline.

All the mentioned works of literature are about optimising the distribution of braking force. However, the regenerated energy depends on several factors such as vehicle speed, vehicle inertia, road, and traffic conditions that were not exhaustively investigated. For instance, the involvement of unintended braking forces may deteriorate drivers' comfort while slowing down vehicle speed. Moreover, the performance of the braking strategies was assessed only in simplified scenarios, which could not directly prove the effectiveness of the strategies.

In order to ensure vehicle safety and improve driving performance under a diverse range of driving conditions, while optimising energy recovery during braking, hierarchical control strategies have been proposed. Guo et al. (2016) developed a bi-level architecture to solve the torque split problem. The outer control layer computes the optimal velocity trajectory by solving a nonlinear time-varying optimal problem. The inner one provides an explicit solution of the optimal torque split ratio and gear shift schedule by combining Pontryagin's minimum principle and numerical methods in the framework of MPC. The performance of the control system was assessed by employing the new European driving cycle (NEDC) and urban dynamometer driving schedule (UDDS). The results indicated that energy efficiency (SOC) and speed trajectories (for inner-city driving cycle) were improved w.r.t. rule-based and DP controllers. To solve the same problem, a feedback hierarchical controller was designed by Chen et al. (2018). Also in this case, the upper-layer tracks the reference speed profile to be imposed on the vehicle, while the lower-layer controller improves the energy recovery by allocating the braking torques among front and rear wheels. However, the speed-tracking and energy consumption performance of the control strategy was compared with a sliding mode controller in two simplified scenarios. Conversely, Li et al. (2021) suggested a three-level control architecture to simultaneously achieve energy saving, route tracking, and dynamics stability. Herein, the top layer embeds some rules to maximise both the energy recovery and control commands; the middle layer serves for imposing the commands to the vehicle in an energy-saving perspective; the bottom layer, instead, focuses on distributing the hydraulic and regenerative toques in an optimal way. The simulation analysis was carried out by means of Carsim, and corner and double-line change scenarios were chosen to test the proposed coordination control strategy. For comparison purposes, a hierarchical scheme, employing an MPC and a Linear Quadratic Regulator (LQR) to track desired speed profile, and I-curve method were used. However, all these aforementioned approaches do not allow for management constraints in an integrated way. Indeed, they do not deal with the problems of hydraulic/regenerative braking torque distribution and front/rear braking distribution in a unified framework. In Table 1 we summarise a comparison of our method with the above-referenced state-of-the-art controllers, where it is clearly highlighted our contributions w.r.t. technical literature.

3. Control-oriented modelling of Autonomous Electric Vehicles

Consider an Autonomous Electric Vehicle, known as the Ego-Vehicle, that uses four in-wheel motors to propel itself along a straight roadway. The Ego-Vehicle is equipped with on-board sensors that measure state variables such as the chassis speed, acceleration, and tire angular speeds. Additionally, ranging sensors, such as cameras and radar, are utilised to determine the relative position and speed of other vehicles or to detect potential obstacles. Furthermore, the Ego-Vehicle is equipped with a regenerative braking system that allows for energy recovery during braking.

3.1. Ego-Vehicle dynamics

In this section we present the control-oriented vehicle model that underlies the design of our double-layer control architecture. The control-oriented vehicle model is based on several assumptions. Firstly, we limit our analysis to the vehicle's longitudinal dynamics, thereby disregarding any roll and pitch motions. Secondly, we neglect the impact of multi-physical effects, such as thermal, wear, and abrasive degradation, on the mechanical components of the vehicle. Thirdly, we model the tire solely in terms of its kinematic-dynamic transfer function. Fourthly, we assume that the vertical load acts on the centre of gravity of the vehicle. Finally, we simplify our analysis by assuming that the behaviour of the left and right parts of the vehicle is similar,

Table 1
Comparison and contributions w.r.t. the related works.

Reference	Work objective	Control strategy	Testing speed profile	KPIs
Zhang et al. (2012)	Trajectory Tracking; Energy Recovery; Ensuring Safety	Rule-Based	Light Braking Speed Profile; New European Driving Cycle	Tracking Performance; State of Charge; Tire Saturation; Regeneration Efficiency
Zhang et al. (2013)	Trajectory Tracking; Energy Recovery; Ensuring Safety	Rule-Based	China Light-Duty Test Cycle	Tracking Performance; State of Charge; Tire Saturation; Regeneration Efficiency
Ko et al. (2014b)	Torque Computation; Energy Recovery	Rule-based	Light Braking Speed Profile	Tracking Performance; Energy Consumption
Kanarachos et al. (2014)	Torque Blending; Energy Recovery	State-Dependent Riccati Equation	Emergency Braking Speed Profile	Tracking Performance; Energy Consumption; State of Charge; Tire Saturation
Lv et al. (2014)	Torque Blending; Energy Recovery	Kalman Filter Based Compensation	Light Braking Speed Profile	Tracking Performance; Regeneration Efficiency
Maia et al. (2015)	Energy Recovery; Ensuring Safety	Fuzzy control	Urban and Suburban Area Speed Profiles	Tracking Performance; State of Charge
Xiao et al. (2017)	Trajectory Tracking; Torque Blending; Energy Recovery; Ensuring Safety	Fuzzy Control NMPC	ShenZhen City Cycle; New European Driving Cycle	Tracking Performance; Blended Torque; Tire Saturation
Basrah et al. (2017)	Trajectory Tracking; Torque Blending; Energy Recovery; Ensuring Safety	MPC; NMPC	Light Braking Speed Profile	Tracking Performance; Blended Torque; Tire Saturation
Xin et al. (2019)	Torque Blending	Fuzzy control	City Cycle Driving Condition	Tracking Performance; Energy Consumption; State of Charge; Blended Torque
Huang and Wang (2012)	Torque Blending; Energy Recovery; Ensuring Safety	Hierarchical NMPC	Light Braking Speed Profile; Emergency Braking Speed Profile	Tracking Performance; Regenerative Energy; Blended Torque
Guo et al. (2016)	Trajectory Tracking; Torque Blending; Energy Recovery	Hierarchical NMPC	New European Driving Cycle; Urban Dynamometer Driving Schedule	Tracking Performance; Energy Consumption; State of Charge; Blended Torque
Chen et al. (2018)	Trajectory Tracking; Torque Computation; Energy Recovery	Hierarchical Rule Based	Light Braking Speed Profile	Tracking Performance; Energy Consumption; State of Charge; Regeneration Efficiency
Li et al. (2018)	Trajectory Tracking; Ensuring Safety	Hierarchical NMPC	Light Braking Speed Profile	Tracking Performance; Tire Saturation; State of Charge
Xu et al. (2019)	Trajectory Tracking; Torque Blending; Ensuring Safety; Energy Recovery	Hierarchical NMPC	Emergency Braking Speed Profile	Tracking Performance; State of Charge; Tire Saturation; Blended Torque
Li et al. (2021)	Trajectory Tracking; Torque Blending; Energy Recovery	Hierarchical NMPC	Corner Condition; Double Line Change Condition	Tracking Performance; State of Charge; Blended Torque
Proposed Energy -Oriented Double Layer Control Architecture	Trajectory Tracking; Torque Blending; Ensuring Safety; Energy Recovery	Hierarchical NMPC	New European Driving Cycle; Emergency Braking Speed Profile	Tracking Performance; Energy Consumption; Total Mileage; Battery Requirement; Expected Energy Saved; Blended Torque

while there are differences between the front and rear sections. Therefore, we introduce the notation $j \in \{f, r\}$ to denote the variables related to the front and rear, respectively. Accordingly, the longitudinal and rotational motion of the Ego-Vehicle can be described via the following non-linear dynamical system (De Castro et al., 2012):

$$m\dot{v}(t) = F_{x_f}(t) + F_{x_r}(t) - F_{res}(t), \tag{1}$$

$$J_j \dot{\omega}_{w_j}(t) = \frac{1}{2}\left(R_w F_{x_j}(t) - T_{w_j}(t)\right), \quad j \in \{f, r\}, \tag{2}$$

where m [kg] is the total mass of the vehicle; R_w [m] is the wheel's radius; $v(t)$ [m/s] is the vehicle longitudinal speed; $F_{x_f}(t)$ [N] and $F_{x_r}(t)$ [N] are the longitudinal tire–road friction force at front and rear tires, respectively; J_j [kg m^2] and $\omega_{w_j}(t)$ [rad/s] are the rotation inertia and the rotary speed of front and rear wheels, respectively; $T_{w_j}(t)$ [Nm] is the total torque on front and rear wheels. $F_{res}(t)$ [N] is the resistance force due to the aerodynamic drag force and the rolling resistance at tires, which depends on vehicle's speed and vertical load on tires,

$F_{z_j}(t)$ [N], as (Guo et al., 2021; Rajamani, 2011)

$$F_{res}(t) = \underbrace{\left(\frac{1}{2}\rho A_v v^2(t) C_d\right)}_{F_{aero}(t)} + \underbrace{\left(c_r\left(F_{z_f}(t) + F_{z_r}(t)\right)\right)}_{F_{roll}(t)}, \tag{3}$$

where ρ [kg/m^3] is the air density, A_v [m^2] is the vehicle frontal area, C_d [−] is the aerodynamic drag coefficient and c_r [−] is the rolling resistance coefficient. Tire–road friction force in (1) and (2) can be computed as the product between the vertical load $F_{z_j}(t)$ and the tire–road friction $\mu_j(\kappa)$ as

$$F_{x_j}(t) = \mu_j(\kappa) F_{z_j}(t), \quad j \in \{f, r\}, \tag{4}$$

being κ the slip ratio.

The vertical load $F_{z_j}(t)$ consists of three components. The first one takes into account the static loads $W_f(t)$ [N] and $W_r(t)$ [N], i.e. the forces acting on axles in a stationary condition ($v(t) = 0$ and $a(t) = 0$), which have a direct dependence on the position of the vehicle body centre of gravity:

$$W_f = \frac{mgl_r}{l_f + l_r}, \tag{5}$$

$$W_r = \frac{mgl_f}{l_f + l_r}, \tag{6}$$

where l_f [m] and l_r [m] are the distances w.r.t. the front and the rear axles from the centre of gravity, respectively.

The second component is the load transfer which, by introducing h [m] as the height of the centre of gravity, is given as

$$\Delta F_z(t) = \frac{mha_x(t)}{l_f + l_r}, \tag{7}$$

where $a_x(t)$ [m/s^2] is the longitudinal acceleration.

The last component is the aerodynamic down-force $F_{aero}(t)$ in (3). In so doing, the vertical load can be computed as follows (Guiggiani, 2014):

$$F_{z_j}(t) = -\left(W_j - \Delta F_z(t) + F_{aero}(t)\right) \quad j \in \{f, r\}. \tag{8}$$

Regarding the tire–road friction coefficient in (4), we exploit the Pacejka's Magic Formula (Pacejka, 2005) to determine the longitudinal force arising from this interaction, i.e.:

$$\mu_j(\kappa) = D_x \sin\left\{C_x \tan^{-1}\left[B_x\kappa_j - E_x\left(B_x\kappa_j - \tan^{-1}(B_x\kappa_j)\right)\right]\right\}, \tag{9}$$

where B_x, C_x, D_x, and E_x represent the stiffness, shape, peak, and curvature coefficients, respectively, and are functions of the tire vertical load, tire slip rate, and tire slip angle. Here we use a typical set of constant Magic Formula coefficients for common dry road conditions, defined by Pacejka (2005) and reported in Table 2. The longitudinal slip ratio κ_j is then derived as the normalised difference between the actual longitudinal speed at the axle of the wheel and the equivalent rotational speed of the tire, i.e.:

$$\kappa_j(t) = \frac{\omega_{w_j}(t) R_w - v(t)}{v(t)}, \quad j \in \{f, r\}. \tag{10}$$

Finally, the torque exerted on front and rear wheels $T_{w_j}(t)$, $j \in \{f, r\}$, in (2) is given by the following relation:

$$T_{w_j}(t) = \begin{cases} g_0 \tilde{T}_{m_j}(t) & \text{in Traction mode} \\ g_0 T_{m_j}(t) + T_{h_j}(t) & \text{in Braking mode} \end{cases} \tag{11}$$

where g_0 is the transmission ratio of the reduction gear; $\tilde{T}_{m_j}(t)$ [Nm] is the traction motor torque at the wheel j; $T_{m_j}(t)$ [Nm] is the braking motor torque at the wheel j; $T_{h_j}(t)$ [Nm] is the braking hydraulic torque acting on the wheel j.

Finally, according to (11), the control signal to be determined depends on the involved operation mode. Specifically, in traction mode, the control signal, which we indicate as $u_t(t)$ are the motor torque at front and rear wheels, i.e.

$$u_t(t) = \begin{bmatrix} \tilde{T}_{m_f}(t) \\ \tilde{T}_{m_r}(t) \end{bmatrix}. \tag{12}$$

In braking mode, instead, the control signal is denoted as $u_b(t)$, and consists of the motor and hydraulic torque at front and rear wheels, i.e.

$$u_b(t) = \left[T_{h_f}(t) T_{h_r}(t) T_{m_f}(t) T_{m_r}(t)\right]^\top. \tag{13}$$

3.2. Ego-Vehicle battery model

The battery system of the Ego-Vehicle is modelled as an equivalent simplified electric circuit, consisting of an internal voltage source E_{oc} [V] connected to two ideal diodes and two inner resistances R_{in}^+ and R_{in}^- ([Ω]), which represent the battery internal discharging and charging resistances. These two parameters are assumed to be piecewise constant functions of the actual value of the battery SOC (Maia et al., 2015). Therefore, the voltage at the terminal of the battery is modelled as

$$V_t = \begin{cases} E_{oc} - R_{in}^+ I_{batt} & \text{if discharging,} \\ E_{oc} - R_{in}^- I_{batt} & \text{if charging.} \end{cases} \tag{14}$$

By indicating with P_{req} the power required at the battery and with n_b the number of cells composing this latter; the battery current I_{batt} can be derived as:

$$I_{batt}(t) = \begin{cases} \dfrac{E_{oc} - \sqrt{E_{oc}^2 - \dfrac{4R_{in}^- P_{req}}{n_b}}}{2R_{in}^-} & \text{if discharging,} \\ \dfrac{E_{oc} - \sqrt{E_{oc}^2 - \dfrac{4R_{in}^+ P_{req}}{n_b}}}{2R_{in}^+} & \text{if charging.} \end{cases} \tag{15}$$

Finally, the SOC of the battery can be computed as follows:

$$SOC(t) = \begin{cases} SOC_0 - \dfrac{1}{C_{batt}} \int_0^t I_{batt}(\tau) d\tau & \text{if discharging,} \\ SOC_0 - \dfrac{\eta_b}{C_{batt}} \int_0^t I_{batt}(\tau) d\tau & \text{if charging,} \end{cases} \tag{16}$$

where C_{batt} [Ah] is the battery capacity while η_b is the recharging efficiency.

3.3. Power-based energy consumption estimation model

To evaluate the energy consumption evaluation of the Ego-Vehicle for a specific drive cycle we leverage the Comprehensive Power-based EV Energy consumption Model (Fiori et al., 2016). This is a quasi-steady backward highly-resolved power-based model providing two outputs, namely: the instantaneous power needed (P_{req}) [W] and the energy consumption (EC, [kWh/km]). These latter outputs are a function of several different variables, such as vehicle kinematics (e.g. instantaneous speed and grade), vehicle characteristics, and operating variables (power of auxiliary systems). Since this is a backward model, its formulation can be derived starting from the power required by the electric motor P_{req} [W], which is computed as:

$$P_{req}(t) = \begin{cases} \left(\tilde{T}_{m_f}(t) + \tilde{T}_{m_r}(t)\right)\omega(t)\dfrac{1}{\eta_d} + P_{acc} & \text{in traction mode,} \\ \left(T_{m_f}(t) + T_{m_r}(t)\right)\omega(t) \cdot \eta_d + P_{acc} & \text{in braking mode,} \end{cases} \tag{17}$$

where η_d is the driveline efficiency; $P_{acc} = 700$ [W] is the accessories energy consumption. Finally, on the basis of (17), the energy consumption EC is computed according to Fiori et al. (2016):

$$EC = \frac{1}{3600000} \int_0^t P_{req}(\tau) d\tau \frac{1}{d_t}, \tag{18}$$

where d_t [m] is the travelled distance.

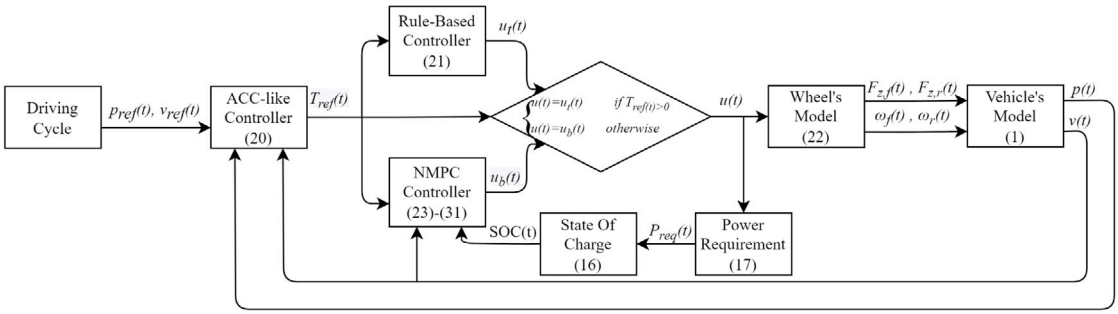

Fig. 1. Double layer control architecture. In each component, block is reported the used equation.

4. Design of the energy-oriented double-layer control architecture

The objective of this study is to devise a new double-layer control architecture for an AEV that can enhance its sustainable behaviour and ensure driving safety in traffic conditions. With this aim in mind, we propose a novel hierarchical control framework for AEVs that can accomplish the following control objectives: (*i*) computing a smooth driving profile that avoids strong acceleration/deceleration manoeuvres while ensuring safety during the travel, i.e. collision avoidance w.r.t. surrounding vehicles; (*ii*) reducing the AEV energy consumption by guaranteeing the tracking of the computed driving profile; (*iii*) maximising energy recovery during braking manoeuvres.

In order to fulfil the aforementioned specifications, the suggested control framework employs an integrated use of ACC-like and NMPC controllers. The high-level controller handles the motion control issue, while the low-level controller deals with the traction control matter. These complementary strategies work in tandem to reduce the overall energy consumption of the AEV, while simultaneously ensuring a safer, more sustainable, and comfortable driving experience. Additionally, this combination is capable of compensating for any efficiency issues arising from external factors, such as traffic conditions encountered by the vehicle. Going into detail, the control strategy exploits the vehicle status information available by using a model-based tire–road friction coefficient technique to compute the blending between hydraulic and motor torque. The first layer consists of a longitudinal ACC-like controller whose purpose is to compute the required traction/braking control signal according to the ACC behaviour, hence imposing a safe and smooth driving profile to the AEV. When in traction mode we exploited the rule-based control in order to split the reference torque between the front and rear wheels. On the other hand, during braking manoeuvres, the desired control signal is set as input to the second layer, consisting of an NMPC strategy that defines the blending between hydraulic and motor torques on front and rear wheels. The blending depends on the vehicle's speed and SOC. Once the control signal has been defined it is used as input to the wheel's model in order to withdraw EV's dynamic. The overall control architecture is disclosed in Fig. 1.

4.1. ACC-like controller design

The longitudinal ACC-like controller is designed to ensure the achievement of the following trajectory-tracking control goals:

$$\lim_{t\to\infty} \|p_{ref}(t) - p(t) - d_{safe}(t)\| = 0, \tag{19a}$$

$$\lim_{t\to\infty} \|v_{ref}(t) - v(t)\| = 0, \tag{19b}$$

where $p_{ref}(t)$ [m] and $v_{ref}(t)$ [m/s] are the position and speed of the ahead vehicle, respectively; $d_{safe}(t) = d_{min} + h_{gap} \cdot v_x(t)$ is the safety inter-vehicle distance in [m], being d_{min} [m] and h_{gap} [s] the standstill distance and the minimum time gap, respectively.

Now, given the position error $e_p(t) = p_{ref}(t) - p(t) - d_{safe}(t)$ and the speed error $e_v(t) = v_{ref}(t) - v(t)$, in order to achieve the control goals in (19) we compute the traction/braking torque via a PID-like control that updates its action based on the errors among information shared by vehicles:

$$T_{ref}(t) = K_P \cdot e_p(t) + K_I \cdot \int_0^t e_p(\tau)d\tau + K_V \cdot e_v(t). \tag{20}$$

The ACC-like controller output $T_{ref}(t)$ [Nm] is the motor control torque used to drive the motion of the vehicle both in traction and braking mode. Specifically, when the vehicle is in traction mode, we split the motor traction at wheels between the front and rear ones as

$$u_t(t) = \begin{bmatrix} \tilde{T}_{m_f}(t) = 0.6 \times T_{ref}(t) \\ \tilde{T}_{m_r}(t) = 0.4 \times T_{ref}(t) \end{bmatrix}. \tag{21}$$

On the other hand, when in braking mode, $T_{ref}(t)$ has to be optimally split between the in-wheel motor and hydraulic torque so to optimise the energy recovery. To this aim, we design an NMPC approach for this braking torque blending.

It is worth noting that the use of an ACC can improve the energy performance of a vehicle because the system constantly monitors the vehicle speed and automatically adjusts its acceleration and deceleration to maintain a safe distance from an ahead vehicle. In this way, the ACC avoids hard braking and sudden accelerations, thus reducing the vehicle energy consumption and increasing its sustainability level.

4.2. NMPC controller design

The second layer of the proposed architecture is based on an NMPC controller aiming at optimising the energy recovery during braking manoeuvres by blending torques (hydraulic and motor pairs) on the front and rear wheels. More specifically, during braking, the ACC-like reference torque $T_{ref}(t)$ is used as reference value to the NMPC, whose objectives are: (*i*) recover as much energy as possible; (*ii*) ensure safety conditions, i.e. avoid collisions with ahead vehicles.

4.2.1. Prediction model

To properly design the NMPC so to take explicitly into account the aforementioned control objectives (see items (*i*) and (*ii*) in Section 1), we firstly recast the control-oriented vehicle model on the basis of (2) and (4). To this purpose, let us introduce the state variables for the prediction model of the NMPC, i.e. the angular speed of the wheels, as $x(t) = [x_1(t),\ x_2(t)]^\top = [\omega_{w_f}(t),\ \omega_{w_r}(t)]^\top$. As consequence, the behaviour of the Ego-Vehicle in (2) can be re-written as

$$\begin{aligned} \dot{x}_1(t) &= \frac{g_0}{J_f}\left[\frac{1}{2}R_w\mu_f(x_1)F_{z_f}(t) - T_{h_f}(t) - g_0T_{m_f}(t)\right], \\ \dot{x}_2(t) &= \frac{g_0}{J_r}\left[\frac{1}{2}R_w\mu_r(x_2)F_{z_r}(t) - T_{h_r}(t) - g_0T_{m_r}(t)\right], \end{aligned} \tag{22}$$

whose discrete form, derived using the Euler method considering k as current time instant and T_s [s] as sample time, is given by:

$$x_1(k+1) = \frac{T_s g_0}{J_f}\left[\frac{1}{2}R_w \mu_f(x_1(k))F_{zf}(k) - T_{h_f}(k) - g_0 T_{m_f}(k)\right] + x_1(k),$$
$$x_2(k+1) = \frac{T_s g_0}{J_r}\left[\frac{1}{2}R_w \mu_f(x_2(k))F_{zr}(k) - T_{h_r}(k) - g_0 T_{m_r}(k)\right] + x_2(k). \tag{23}$$

4.2.2. Cost function

To achieve the control objectives defined in Section 4.2, we compute the control signal $u_b(t)$ in (13) by solving the following multiple-objective nonlinear constrained optimisation problem:

$$\min_{U_k} J(x(k), U_k, \delta) = \min_{U_k}(J_1 + J_2 + J_3 + J_4) \tag{24}$$

subject to

$$x(k+1) = f(x(k), u(k))$$
$$0 \le v(k) \le v_{max}$$
$$a_{min} \le a_x(k) \le a_{max}$$
$$T_{m_f}(k) + T_{m_r}(k) \ge \mathcal{T}_m(k)$$
$$\delta(k) = \begin{cases} 1 & \text{if } SOC(k) < 85\% \\ 0 & \text{if } SOC(k) \ge 90\% \text{ or } \omega \ge \omega_c \\ \delta(k-1) & \text{if } 85\% < SOC(k) < 90\% \end{cases}$$

where $f(x(k), u(k))$ is the non-linear dynamic (23), U_k is the dependent variable i.e. the optimal sequence of the control variable $u_b(k)$, which is described as $U_k \stackrel{\text{def}}{=} \{u_b(k|k), u_b(k+1|k), \dots, u_b(k+\theta-1|k)\}$, being θ the prediction horizon; $v_{\max}$ [m/s] is the maximum speed that Ego-Vehicle can reach; a_{min} [m/s^2] and a_{max} [m/s^2] are the minimum and maximum longitudinal acceleration; $\mathcal{T}_m(k)$ [Nm] is the time-varying limitation on the braking motor torque. Specifically, it represents the maximum deliverable torque, which decreases as the wheel angular speed grows according to the following non-linear relationship:

$$\mathcal{T}_m(k) = \begin{cases} T_{m,min}, & \omega_m(k) \le \dfrac{P_{m,max}}{|T_{m,min}|} \\ \dfrac{P_{m,max}}{\omega_m(k)}, & \omega_m(k) > \dfrac{P_{m,max}}{|T_{m,min}|} \end{cases} \tag{25}$$

being $T_{m,min} = -300$ [Nm] the minimum motor torque that can be delivered based on the characteristics of the vehicle and $P_{m,max} = 2.6$ [kW]. Finally, $\delta(k)$ is a discrete variable introduced to improve the energy-saving performance of the proposed NMPC-based control and initialised to 1. It is designed to guarantee that energy regeneration is enabled until the $SOC < 90\%$. To avoid battery overcharging, regeneration is disabled when the aforementioned threshold is reached or when the wheel speed of the vehicle is such that the regeneration cannot take place (i.e. $\omega \le \omega_c$ ($\sim$15 [rad/s])). Regarding the cost function reported in (24), each term is purposely designed to achieve a different control objective. The first and the fourth terms are designed for ensuring braking safety and tracking of the reference speed profile, while the second and third ones are designed for improving regeneration efficiency. The first term J_1 aims at ensuring optimal tracking of the reference braking torque $T_{ref}(k)$ computed by the ACC-like controller. In other words, this quadratic term allows tracking of the reference braking profile while ensuring braking safety:

$$J_1 = Q\sum_{i=1}^{\theta}\Big[2\left(T_{h_f}(k+i|k) + T_{h_r}(k+i|k)\right)r + 2g_0\delta(k)\left(T_{m_f}(k+i|k) + T_{m_r}(k+i|k)\right) - T_{ref}(k)\Big]^2, \tag{26}$$

where Q is the factor that weights how J_1 contributes to the overall cost function J.

The second term J_2 of the cost function is a penalty term for the total mechanical power of four in-wheel motors. More specifically, it is designed to recover energy as much as possible:

$$J_2 = S\sum_{i=1}^{\theta}\left[-2\delta(k)\left(T_{m_f}(k+i|k)\omega_{m_f}(k+i|k) + T_{m_r}(k+i|k)\omega_{m_r}(k+i|k)\right)\right], \tag{27}$$

where S is the corresponding weighting factor.

The third term J_3 is is designed to minimise the energy consumption due to the hydraulic braking mode. Specifically, it aims at minimising the total mechanical power of the hydraulic unit , hence maximising the usage of the regenerative braking:

$$J_3 = T\sum_{i=1}^{\theta}\left[\frac{2}{g_0}\left(T_{h_f}(k+i|k)\omega_{m_f}(k+i|k) + T_{h_r}(k+i|k)\omega_{m_r}(k+i|k)\right)\right], \tag{28}$$

where T is the corresponding weighting factor.

The fourth term J_4 of the cost function focuses on the cooperative control of the front and rear braking, which is critical for vehicle braking performance and safety. Here we assume that the relationship between the front and rear braking forces follows the so-called ideal braking force distribution, or I-curve, hence allowing the front and rear axles to simultaneously lock. In so doing, this term aims to make the actual front and rear braking force distribution close to the ideal distribution, hence maximising the stability of the vehicle during braking (Genta and Morello, 2019). To derive this last term, let first consider the total braking force of the vehicle described as

$$F_x(k) = \mu(k)Mg = F_{x_f}(k) + F_{x_r}(k). \tag{29}$$

Following the approach proposed by Xiao et al. (2017), this latter function can be expressed as:

$$f(F_{x_f}(k), F_{x_r}(k)) = \frac{1}{2}\left[\frac{mg}{h}\sqrt{l_r + \frac{4h}{mg}F_{x_f}} - \left(\frac{mgl_r}{h} + 2F_{x_f}\right)\right] - F_{x_r} = 0. \tag{30}$$

Accordingly, the fourth term of the cost function is expressed as:

$$J_4 = R\sum_{i=1}^{\theta}\left[\frac{1}{2}\left[\frac{mg}{h}\sqrt{l_r + \frac{4h}{mg}F_{x_f}(k+i|k)} - \left(\frac{mgl_r}{h} + 2F_{x_f}(k+i|k)\right)\right] - F_{x_r}(k+i|k)\right]^2, \tag{31}$$

where R weights the contribution of J_4 to J.

5. Validation scenario and key performance indexes

Within this section, we provide an overview of the simulation configuration and the performance metrics employed to assess the effectiveness of the suggested control approach in improving the energy-recovery performance of the Ego-Vehicle. Simultaneously, we ensure that the system meets the prescribed tracking and safety requirements.

Extensive simulation analysis is carried out by leveraging MiTraS platform (Bifulco et al., 2022), which allows emulating the realistic nonlinear vehicle dynamics (not explicitly considered in the control design phase) as in Pariota et al. (2020). Herein, we also incorporate accurate modelling of response delay and imperfect executions of the vehicle's mechanical systems. As the vehicle's ability to execute the desired traction/braking torque, as per the control strategy, significantly impacts its motion, it is crucial to examine the robustness of the control approach using detailed non-linear vehicle dynamics.

Moreover, in real-world scenarios, a multitude of disparities exist between the actual plant and the control-oriented model, which unavoidably arise due to factors such as vehicle technology, vehicle dynamics, road features, and usage conditions. As these mismatches have a significant impact on the efficacy of a control strategy, we investigate the effect of uncertain parameters on the performance of the proposed

Table 2
Nominal parameters of the Ego-Vehicle model and corresponding considered range (uncertainty).

Parameter	Symbol	Value	Uncertainty
Vehicle Mass	m	1520 [kg]	±20%
Driveline efficiency	η_d	0.89 [–]	±5%
Wheel Radius	R_w	0.29 [m]	±2%
Drag coefficient	C_d	0.30 [–]	±10%
Frontal area	A_v	2.2 [m^2]	±10%
Air Density	ρ	1.2256 [kg/m^3]	–
Distance c.o.g. - front axle	l_f	0.9 [m]	–
Distance c.o.g. - rear axle	l_r	1 [m]	–
Height c.o.g.	h	0.25 [m]	–
Wheel Moment of Inertia	J	1 [kg/m^2]	–
Gear Reduction	g_0	5 [–]	–
Battery capacity	C_{batt}	65 [Ah]	–
Recharging Efficiency	η_b	0.9 [–]	–
Number of Battery Cells	n_b	96 [–]	–
Magic Formula	B_x, C_x	10 [–], 1.9 [–]	–
Parameters	D_x, E_x	1 [–], 0.97 [–]	–

double-layer controller. The Ego-Vehicle parameters are reported in Table 2, among which 5 parameters are assumed to be uncertain with their own range of variability, i.e. the percentage deviation of the actual value from the nominal one. The interval bounds are selected based on physical or operating constraints set by vehicle dynamics (Fiori et al., 2020).

To evaluate the performance of the Ego Vehicle under the action of the proposed control architecture, for all possible combinations of the unknown time-varying parameters, which are assumed to be uniformly distributed, we employ the LHS approach (Helton and Davis, 2003) to generate a near-random sample of 30 parameter values from a multidimensional distribution. Regarding the battery system parameters, they are also reported in Table 2 while the piece-wise constants R_{in}^{+} and R_{in}^{-} defined in Section 3 are stored in a lookup table whose values are selected according to Maia et al. (2015).

Control gains parameters for the ACC-like controller in (20) are tuned (according to Theorem 1 in Manfredi et al. (2020)) as $K_P = 100$, $K_I = 10$ and $K_V = 400$.

In regard to the weighting factor employed in the NMPC optimisation problem (24), we investigate two distinct sets of weights for the cost function. Since the proposed NMPC involves a multi-objective optimisation problem, where the cost function is a combination of various performance metrics, the adjustment of weights enables the determination of the relative significance of each control objective within the cost function. The selection of weight factors is carried out by exploiting a trial-and-error approach as detailed by Cortés et al. (2009).

The main difference between those relies on how much the cost functions (26) and (31) are weighted w.r.t. to the other two, namely: NMPC-1 gives high priority to the tracking (J_1 and J_4) by giving up some regenerative potential (J_2 and J_3), i.e. we choose $Q = 10$, $S = 2$, $T = 2$, $R = 12$; on the other hand, NMPC-2 gives higher priority to energy recovery by weighting less the cost functions J_1 and J_4, while the ones related to J_2 and J_3 remain constant i.e. $Q = 5$, $S = 2$, $T = 2$, $R = 7$. Employing values of $Q_{\text{NMPC-1}} > Q_{\text{NMPC-2}}$ and $R_{\text{NMPC-1}} > R_{\text{NMPC-2}}$, while keeping the other weights unchanged, this lead to reduced tracking error for NMPC-1. On the other hand, i.e. with NMPC-2, the weight selection increases the energy saving.

To appraise the energy and tracking capabilities of the proposed double-layer control architecture in the presence of model parameter uncertainties, we consider the following Key Performance Indexes (KPIs):

(i) speed profile [m/s];
(ii) inter-Vehicle distance [m];
(iii) Tracking Index (TI) defined by Wu et al. (2019)

$$TI = \frac{1}{T}\int_0^T (|e_v(t)\cdot SDE + e_p(t)\cdot SVE|)dt\,, \tag{32}$$

being T [s] the simulation length while SVE and SDE are the sensitivity to the velocity error and distance error;
(iv) average Consumption [kWh/km] as in (18);
(v) SOC [%];
(vi) Hydraulic and Motor Torque [Nm];
(vii) energy reduction.

For the investigation of energy consumption reduction, utilising the knowledge of battery characteristics, we compute the energy required for travel, both with and without the optimal proposed energy recovery, in terms of battery capacity as

$$C_{red} = Mil_{base}(EC_{reg} - EC_{base}), \tag{33}$$

where EC_{reg} [kWh/km] is the energy consumed by the energy-oriented control strategies while EC_{base} is the energy required for travelling without considering our energy regeneration policy; furthermore we define Mil as the total mileage [km] per charge, expressed as:

$$Mil = \frac{C_{batt}(n_b \cdot V_b)}{EC}, \tag{34}$$

therefore Mil_{reg} and Mil_{base} will be the total mileage with and without regeneration respectively obtained by adapting EC (EC_{reg} or EC_{base}) in (34).

Finally, we also consider as energy KPI the total expected energy saved by regenerative braking control strategy in the whole life cycle which can be computed as:

$$E_{save} = Mil_{bat}\frac{(Mil_{reg} - Mil_{base})}{\eta_b}. \tag{35}$$

where Mil_{bat} is the lifetime mileage of the battery.

To demonstrate the energy-saving benefits of the proposed control architecture, we compare its performance with other state-of-the-art control strategies, namely: **(1)** a PI controller, referred to as the base controller, which lacks regenerative effects and simply imposes the reference torque computed by the ACC-like layer without optimisation during the braking phase; **(2)** a rule-based regenerative braking control strategy that ensures the same constraints as the proposed double-layer control strategy and splits the reference torque, obtained from the first layer, based on the rules proposed in Ko et al. (2014a); **(3)** the NMPC-based hierarchical control architecture, referred to as *NMPC-C* (where C refers to comparison), proposed in Li et al. (2021). Note that, for the sake of comparison fairness, these control strategies **(1)**, **(2)**, and **(3)** present the same subdivision of the torque to the wheels as in (21).

6. Performance analysis

In what follows, we analyse the effectiveness of the proposed optimal energy-recovery double-layer control architecture, for both the appraised configuration NMPC-1 and NMPC-2, in the following two traffic scenarios:

(a) New European Driving Cycle (NEDC);
(b) hard braking manoeuvre.

In the Scenario **(a)** the Ego-Vehicle follows the NEDC drive cycle to test both the tracking and energy-saving efficiency of the proposed control architecture. Indeed, multiple acceleration and deceleration manoeuvres occur during the 1180 [s] of simulation; therefore it is possible to evaluate the behaviour of the Ego-Vehicle both in braking and traction mode. Conversely, in Scenario **(b)** we consider that Ego-vehicle has to perform a sudden braking manoeuvre which is essential to properly evaluate if the safety requirement is achieved by the controller. For both scenarios, the adhesion coefficient of the road is

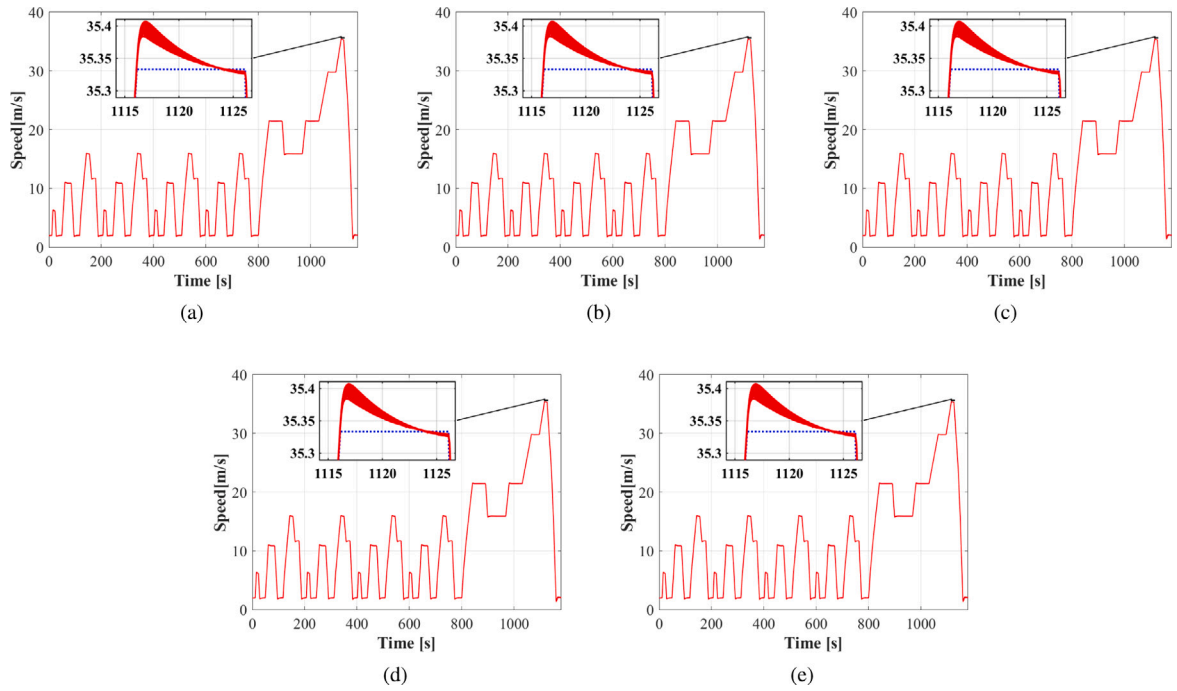

Fig. 2. Speed Tracking performance for NEDC drive cycle. Robustness analysis via the Latin Hypercube Sampling Method. Time history of: (a) PI controller; (b) Rule-based controller; (c) NMPC-C; (d) NMPC-1; (e) NMPC-2.

assumed to be equal to 0.85 (dry condition) and the initial SOC of the battery is set at 85%.

6.1. NEDC

To accurately evaluate the efficiency and efficacy of a blended braking system for electric vehicles, it is essential to determine the amount of energy consumed during braking. To accomplish this, we utilise the findings of Ruan et al. (2016), who assess the energy consumption distributions across various typical driving cycles for a medium-sized passenger Battery Electric Vehicle (BEV), without regenerative braking.

Among all the possible drive cycles, we select the NEDC for which the energy wasted during braking is 28% so that we can assess the potential energy saving of our approach. The NEDC drive cycle is based on traffic data from European capitals (Paris and Rome) (Tzirakis et al., 2006) and represents the typical usage of a car in Europe. It is purposely designed to assess the environmental footprint of passenger cars. It consists of four repeated ECE-15 Urban Driving Cycles and one Extra-Urban Driving Cycle. Specifically, the urban part has a total duration of 780 [s] over a distance of 3976.1 [m], with an average speed of 18.35 [km/h]. On the other hand, the extra-urban part represents more aggressive and high-speed driving modes. It has a total duration of 400 [s] over a distance of 6956 [m] and an average speed of 62.6 [km/h]. In this scenario, we assume that the Ego-Vehicle follows an ahead vehicle travelling according to the NEDC speed profile while maintaining a safe inter-vehicle distance of 15 [m].

6.1.1. Tracking performance results

Results related to speed-tracking are reported in Fig. 2 and show that the reference speed is always chased for each considered control strategy. Moreover, although the presence of uncertain vehicle dynamics parameters, the performances do not degrade, proving that each controller succeeds in providing the required torque. Similarly, the position-tracking performance results (Fig. 3) disclose how the distance kept by the Ego-Vehicle never exceeds a maximum error of 0.9 [m], therefore the safety requirement is always ensured during the driving cycle.

To comprehensively quantify tracking capability, we compute the TI for the Ego vehicle as in (32) for each of the 30 simulations performed. The distributions of the index for the employed control strategies are then compared using boxplots. Boxplot is a method for graphically demonstrating the locality, spread and skewness of data through their quartiles, without making any assumptions about the underlying statistical distribution. Results in Fig. 4 confirm the good tracking performance achievable via all the considered controllers but also highlight a slight improvement of tracking performance achievable via our double-layer control approach for both the appraised configurations (the median value, i.e. the red line in the box, is shifted towards lower values). Specifically, regarding the median behaviour, results show a 6.29% and a 4.5% improvement of the TI while using the two operating configurations of the NMPC respectively w.r.t. the PI control strategy; furthermore, w.r.t. the rule-based control, we evaluated a 4.8% and a 2.98% improvement of the TI; finally an improvement of 3.02% and 1.17% is appreciable w.r.t. the NMPC-C. Furthermore, it is interesting to note and compare the performance of the proposed NMPC in the two different configurations. Indeed, NMPC-1 results in a 1.78% performance increment w.r.t. NMPC-2. This slight improvement in the tracking performance is due to different weights in the cost function J in (26). More specifically, the NMPC-1 gives higher priority to tracking performance w.r.t. NMPC-2 since $Q_{\text{NMPC-1}} > Q_{\text{NMPC-2}}$. By weighting more the tracking term J_1 in (26), the control signals computed by the NMPC-1 controller minimise the tracking error. The outcome in Fig. 4(a) shows also a variation in the TI distribution. Note that the standard deviation is a measure of the amount of variation of a set of values; hence, a reduction of this term implies an increase in the homogeneity of vehicle behaviour in the presence of uncertain parameters. Specifically, using the PI control strategy, the standard deviation is 0.0758, while using the rule-based control and NMPC-C it is slightly reduced (0.0747 and 0.0674, respectively). Lastly, NMPC-1 and NMPC-2 allow a reduction of the standard variation, which is equal to 0.0723 and 0.0749 respectively. Similarly to what was obtained for the median, the whole distribution of NMPC-1 is shifted towards lower values than NMPC-2. That is, the NMPC-1 achieves better tracking performance w.r.t. NMPC-2.

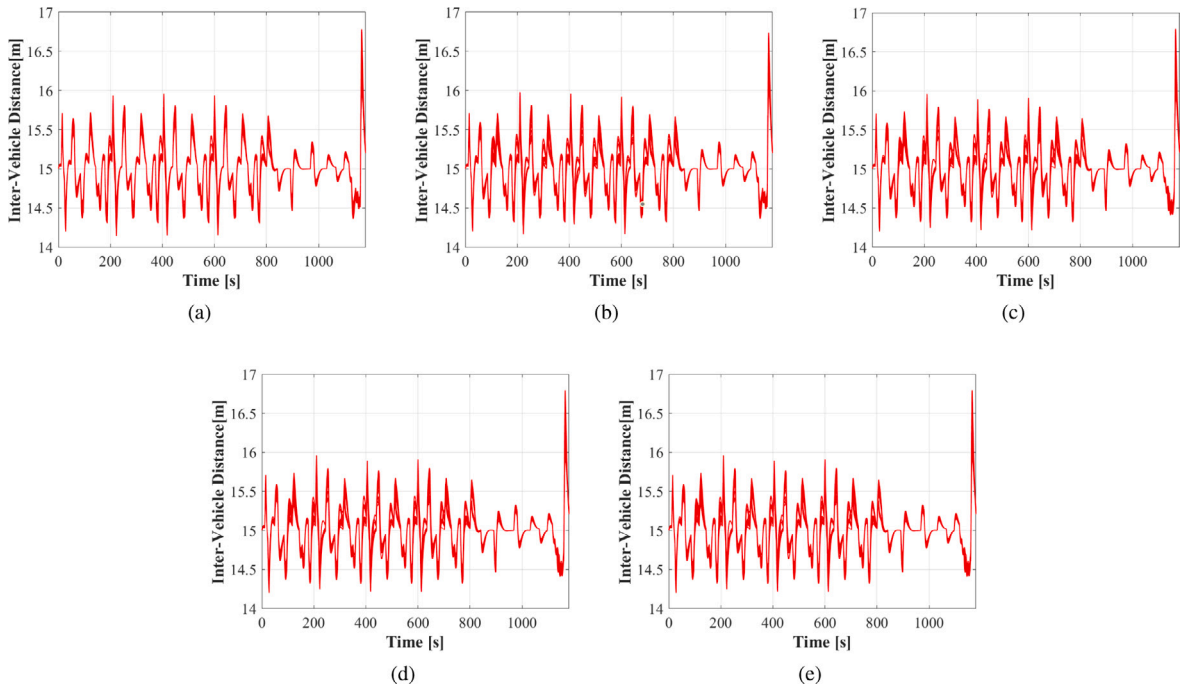

Fig. 3. Inter-Vehicle distance performance for NEDC drive cycle. Robustness analysis via the Latin Hypercube Sampling Method. Time history of: (a) PI controller; (b) Rule-based controller; (c) NMPC-C; (d) NMPC-1; (e) NMPC-2.

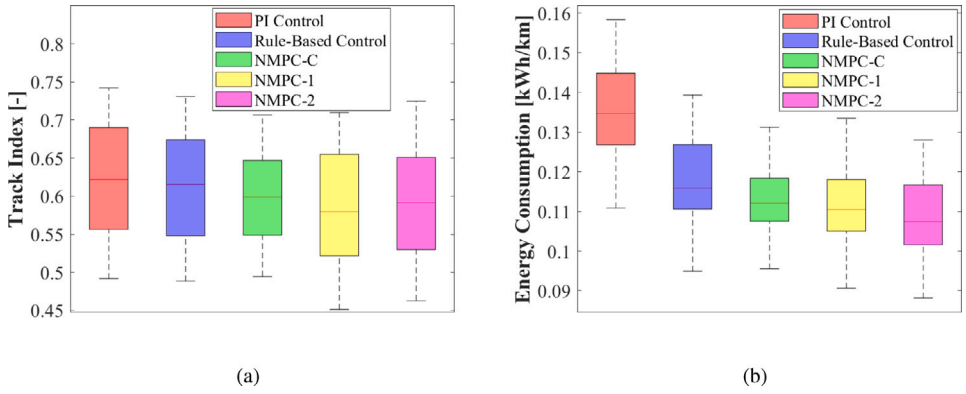

Fig. 4. Comparison analysis for NEDC driving scenario in presence of uncertain vehicle parameters: (a) Track Index; (b) Energy consumption.

Table 3
Energy consumption comparison among different control strategies for NEDC drive cycle. Percentage reduction.

Control strategy	Rule-based	NMPC-C	NMPC-1	NMPC-2
PI control	12.3%	16.8%	17.9%	19.9%
Rule-Based control	–	4.2%	6.3%	8.6%
NMPC-C	–4%	–	1.8%	4.6%

6.1.2. Energy consumption results

Regarding energy consumption, the outcomes prove how the proposed double-layer control strategy allows for improving energy-saving performance. Box-plot results in Fig. 4(b) show a strong reduction of the energy consumption for Ego-Vehicle equipped with the NMPC-based optimised braking strategy w.r.t. the PI, the rule-based and NMPC-C ones. Specifically, by observing comparison results related to average energy consumption reduction in Table 3, it is possible to observe a reduction of 17.9% and 19.9% w.r.t. PI controller, 6.3% and 8.6% w.r.t. rule-based controller and 1.8% and 4.6% w.r.t. the NMPC-C for the first and second operating configuration of the NMPC, respectively. It is interesting to investigate and compare the different performances achieved by NMPC-1 and NMPC-2. Specifically, in this case, a lower value of the tracking term ($Q_{NMPC-2} < Q_{NMPC-1}$) drives the NMPC-2 to manipulate the control signals to improve the energy response. Accordingly, the NMPC-2 reduces consumption of about 2.9% w.r.t. solution NMPC-1. Regarding the dispersion of the obtained distribution, the standard deviation is 0.0111 [kWh/km] for both the baseline PI and the rule-based control strategy. Through the NMPC-C the standard deviation is 0.0078 [kWh/km]. Instead, using the NMPC-based double-layer control architecture, it is possible to obtain more homogeneous results: the standard deviation is 0.0091 [kWh/km] for the NMPC-1, while it is 0.0101 [kWh/km] for the NMPC-2. Finally, similarly to what was obtained for the median, the whole distribution of NMPC-2 is shifted towards lower values than NMPC-1; That is, NMPC-2 allows to achieve better energy-saving performance w.r.t. NMPC-1.

Furthermore, we also report the SOC behaviour (Fig. 5) that confirms the above-explained results. Indeed, the energy-oriented NMPC affects the behaviour of the SOC by discharging the battery slower than the other comparison control strategies: due to torque blending, the

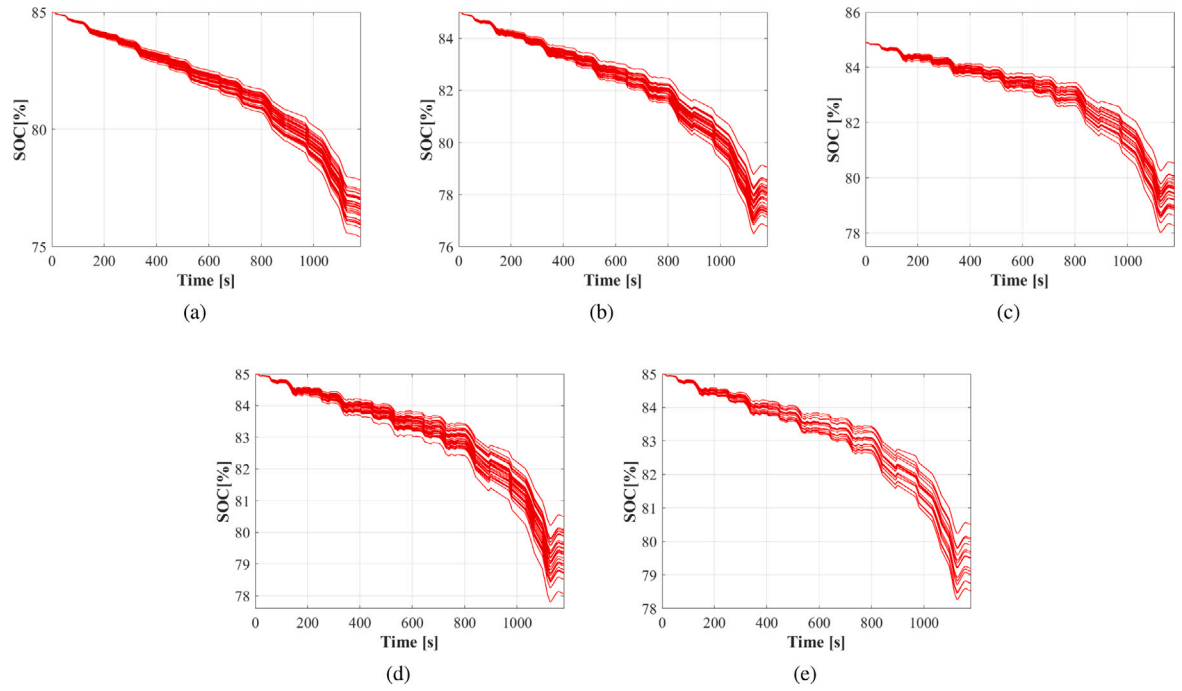

Fig. 5. State-of-Charge performance for NEDC drive cycle. Robustness analysis via the Latin Hypercube Sampling Method. Time history of: (a) PI controller; (b) Rule-based controller; (c) NMPC-C; (d) NMPC-1; (e) NMPC-2.

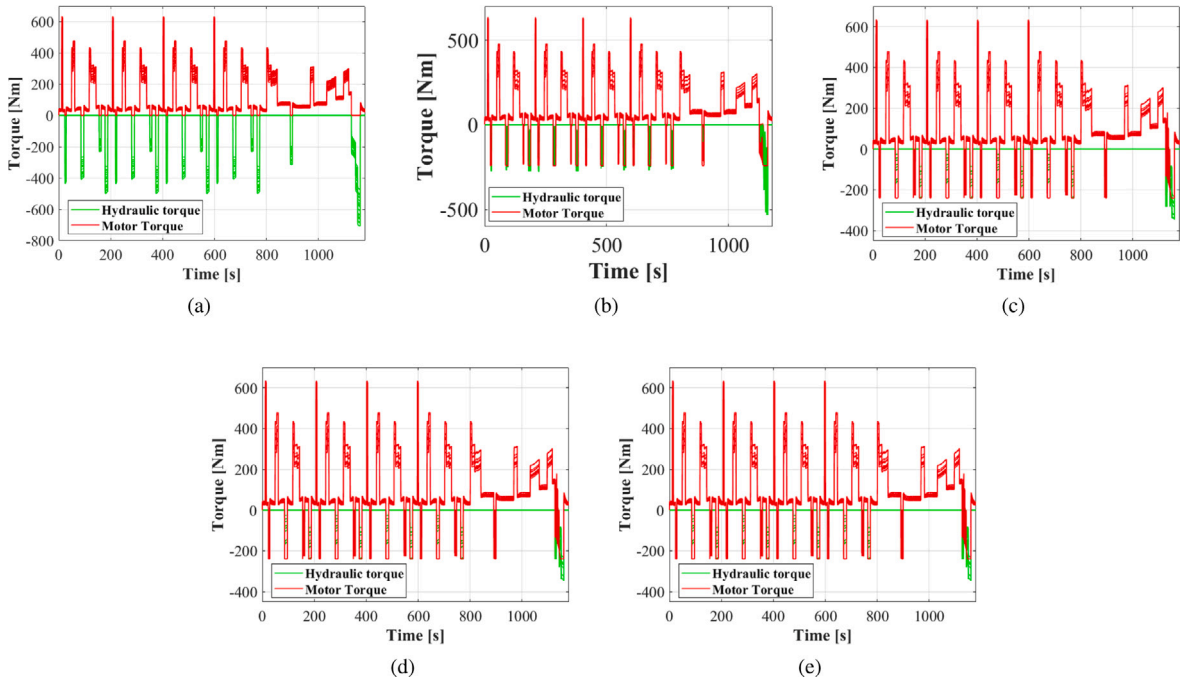

Fig. 6. Hydraulic and motor torque performance for NEDC drive cycle. Robustness analysis via the Latin Hypercube Sampling Method. Time history of: (a) PI controller; (b) Rule-based controller; (c) NMPC-C; (d) NMPC-1; (e) NMPC-2.

Ego-Vehicle can recover much more energy during braking manoeuvres. The SOC percentage undergoes an increment of 3.1% on average when using the NMPC control w.r.t. the base case, 1.6% compared to the rule-based control and 0.7% w.r.t. the NMPC-C.

In Fig. 6 we report the hydraulic and motor torques applied to the wheels for the 4 control schemes considered. Note that, only the behaviour of the different control schemes during braking phases is disclosed since in traction mode their behaviour is similar in all the cases considered. The PI control strategy results in Fig. 6-(a) show that this control strategy does not consider the energy-recovery function; indeed, during braking phases, the torque requirement is fulfilled by the hydraulic torque only. From the rule-based method results shown in Fig. 6-(b), it is possible to see how the strategy allows splitting the required driving torques between the hydraulic and motor torques. However, it is worth noting that the hydraulic torque tends to reach values greater than the motor ones; on the other hand, in the urban part, the hydraulic torques slightly exceed the motor ones, during the extra-urban part this gap increases. Regarding the proposed NMPC,

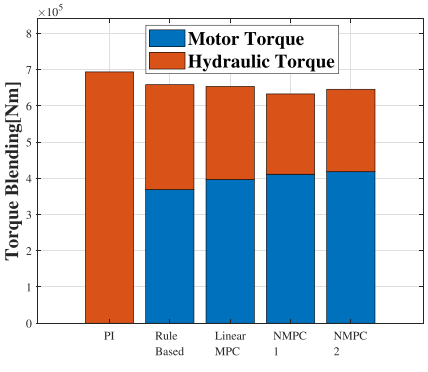

Fig. 7. Motor and hydraulic braking torque distribution for the four control strategies.

in both operating configurations, it allows using the motor braking torque at its maximum potential in the urban part without exceeding the value of the hydraulic counterpart. This is strongly related to the fourth term of the cost function (i.e. (31)), which makes the torque distribution applied to the wheels always lay on the I-curve, maximising the efficiency. In the extra-urban part of the drive cycle, the Ego-Vehicle reaches such a speed that $T_{m,max,eff} < T_{m,max}$; therefore, the Ego-Vehicle has to decelerate to let the hydraulic braking torque reach its maximum value. In this case, the difference between hydraulic and motor torques is strongly reduced compared to the other two control schemes. Moreover, in Fig. 7 we report a bar chart of the average total hydraulic and motor torques used while braking. It can be appreciated a 15.06% (1.98%) increment of the motor torque when using the NMPC in operational configuration 1 w.r.t. the rule-based (NMPC-C) approach and a 17.80% (2.88%) increment in operational configuration 2. Moreover, there is a general improvement of the behaviour of the Ego-Vehicle during braking manoeuvres since the total torque goes down by 1.92% and 0.92% w.r.t. the NMPC-C for operating configurations 1 and 2, respectively, while w.r.t the rule-based control the reduction is about 10.14% and 8.70%, respectively. It is worth noticing that the two operating configurations of the proposed NMPC produce similar results in terms of speed and position tracking, while a slight reduction of energy consumption is given by the second NMPC operating configuration.

Boxplot results in Fig. 8-(a) shows the distribution of mileage obtained employing the different control strategies. As expected, both NMPC operating configurations overperform the other control strategies. Therefore, it is possible to compute the rate of extended mileage per charge for the electric Ego-Vehicle equipped with regenerative braking w.r.t. the PI-control strategy used as a baseline. The presence of a simple energy-saving oriented control strategy (rule-based one) allows for an increase in the total mileage of the Ego-Vehicle (up to about 12%). By using a more sophisticated control architecture as the NMPC-C, higher values of such increments can be obtained, i.e. 19%. Concerning our control strategy, the NMPC-1 allows increasing the total mileage of the Ego-Vehicle up to 22%, while NMPC-2 returns up to 25%.

In terms of battery capacity requirements, the benefits deriving from the reduction of energy consumption can be expressed exploiting (33). Results are reported in Fig. 8-(b). The PI supplies an average mileage of 195 [km], the rule-based method has an average value of 218 [km] while the NMPC-C supplies 231 [km]. The two NMPCs allow up to 238 [km] and 244 [km] on average. Regarding the battery requirements reduction, the average decrements w.r.t. to PI controller are: 5.5 [kWh] for the rule-based controller, 7.9 [kWh] for NMPC-C, 8.5 [kWh] for NMPC-1 and 9.6 [kWh] for NMPC-2.

Along the same line, we compute the total expected energy saved by regenerative braking control strategies in the whole life cycle of the battery using (35) where we assumed $Mil_{bat} = 250,000$ [km] The result shown in Fig. 8-(c) proves once again how the proposed energy-saving oriented control strategy allows, in both operational configurations, to reduce the energy consumed by the vehicle during its whole life cycle. Indeed, the total expected electricity energy saved by regenerative braking control strategies w.r.t. to PI controller are: 8561 [kWh] for the rule-based controller; 12719 [kWh] for NMPC-C; 13262 [kWh] for NMPC-1; 15090 [kWh] for NMPC-2.

These latter results are crucial since the limited electricity energy in the battery can be replenished by regenerative braking, hence it is possible to significantly reduce the battery-related cost by reducing the required capacity of the power source.

It is worth noting that all these outcomes are completely in line with results in Section 6.1.2. Indeed, they confirm the ability of the proposed control strategy (equipped with NMPC-1 or NMPC-2) in improving the energy performance of the electric Ego-Vehicle w.r.t. other approaches.

6.2. Emergency braking

The emergency braking scenario is utilised to ensure that the proposed double-layer control strategy consistently meets the safety requirements. To this end, we examine a representative scenario wherein the preceding vehicle initiates an emergency braking manoeuvre, starting from an initial speed of 20 [m/s], with a deceleration of 5 [m/s^2]. Considering a desired inter-vehicle distance of 15 [m], the Ego-Vehicle must safely come to a complete stop, without colliding with the preceding vehicle. The proposed controller, in both the operational configurations, can chase the speed reference — see Figs. 9-(a) and 9-(b) – while avoiding collisions with the vehicle ahead – see Figs. 9-(c) and 9-(d). The presence of uncertain parameters affects the performance of the Ego-Vehicle in completing the braking manoeuvre since the inter-vehicle distance, at the end of the manoeuvre, varies within a range of ∼0.75 [m] and ∼1 [m], for the first and the second configuration of the NMPC, respectively. However, although there is a slight decrease in the

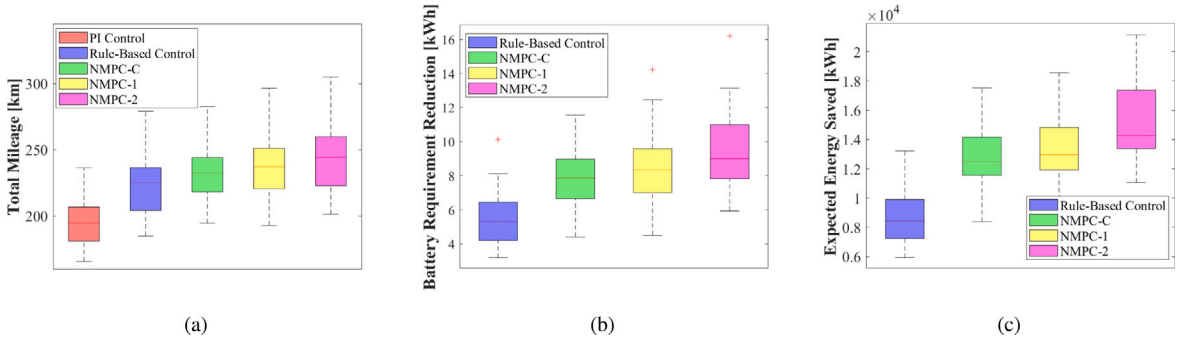

Fig. 8. Comparison analysis for NEDC driving scenario in presence of uncertain vehicle parameters: (a) Average mileage; (b) Battery Requirement Reduction; (c) Total expected energy.

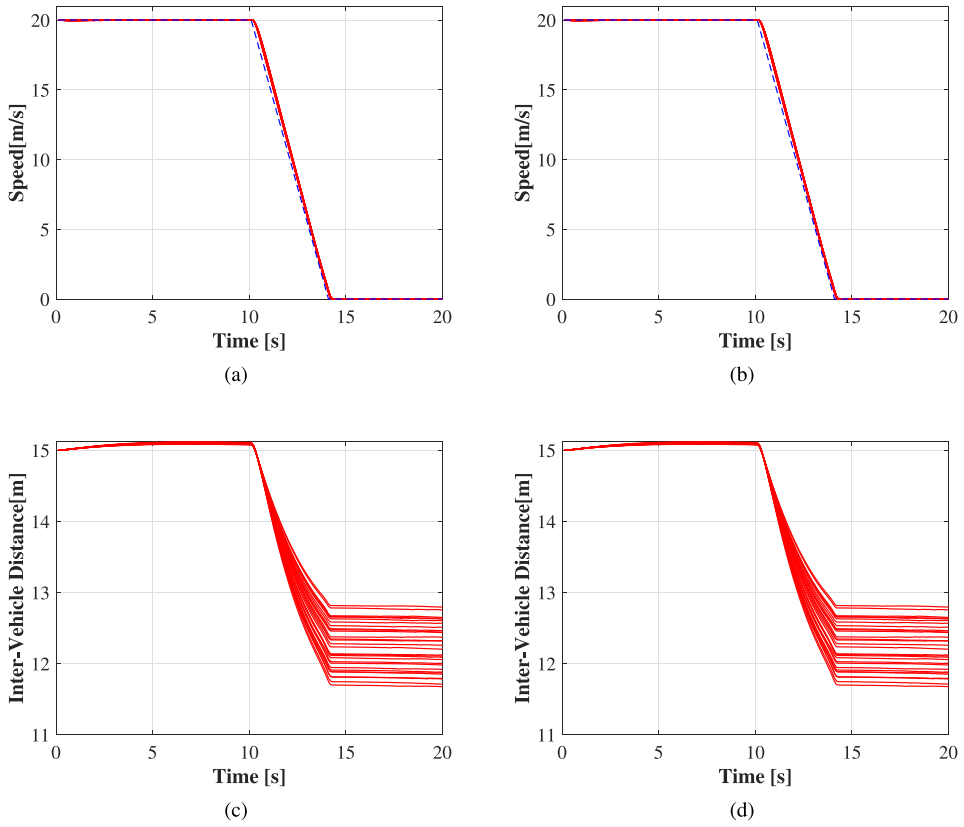

Fig. 9. Emergency braking manoeuvre. Robustness analysis via the Latin Hypercube Sampling Method. Time history of: (a) vehicle speed with NMPC-1; (b) vehicle speed with NMPC-2; (c) inter-vehicle distance with NMPC-1; (d) inter-vehicle distance with NMPC-2.

relative distance w.r.t. the desired one (15 [m]), the two cars are always far enough apart so that the danger can be considered nonexistent and, accordingly, no collision occurs.

7. Conclusions

This study presents a novel double-layer architecture for the longitudinal energy-saving oriented motion control of an electric vehicle, equipped with a regenerative braking system. The first layer of this architecture comprises a PI controller that computes the required traction/braking torque to achieve speed and position tracking requirements. The second layer is activated during braking phases and involves an NMPC controller, which aims to optimise the torque blending between hydraulic and motor braking torques. This approach improves both vehicle stability and potential energy recovery, resulting in enhanced regeneration efficiency.

The effectiveness of the proposed control strategy has been numerically evaluated using the MiTraS simulation environment, while the LHS method was employed to design the experimental campaign considering certain vehicle parameters to be uncertain. Two different scenarios have been defined to test the control algorithm: the NEDC driving cycle to evaluate both tracking and energy-saving performance and the emergency braking manoeuvre to verify the fulfilment of the safety requirement. Additionally, a comparative analysis of alternative control approaches for the NEDC scenario was conducted.

The numerical results obtained from the NEDC drive cycle have revealed that the proposed control strategy exhibits good leader-tracking performance, even in the presence of parameter uncertainties, outperforming the alternative strategies. With regards to energy consumption, the proposed controller is highly effective in reducing the electric vehicle's energy consumption, thus leading to an increase in the total mileage that can be covered per battery charge cycle.

Given the holistic nature of the architecture, having addressed both safety and optimal torque blending for achieving ideal regenerative potential, the method sets the basis for future implementations of regenerative braking control systems. On top of that, having addressed the problem of uncertainty, the architecture has a high potential of being replicated in similar frameworks. Future works could include the possibility to adapt control gains by exploiting meta-heuristic optimisation methods such as Grey Wolf (Cappiello et al., 2021), the exploitation of a more detailed vehicle dynamics model, hardware-in-the-loop testing, and the extension of the methodology to electric platooning applications.

CRediT authorship contribution statement

Angelo Coppola: Conceptualization, Methodology, Software, Formal analysis, Investigation, Validation, Writing – original draft, Writing – review & editing. **Gianmaria De Tommasi:** Conceptualization, Methodology, Software, Formal analysis, Investigation, Validation, Writing – original draft, Writing – review & editing, Supervision. **Carlo Motta:** Conceptualization, Methodology, Software, Formal analysis, Investigation, Validation, Writing – original draft, Writing – review & editing. **Alberto Petrillo:** Conceptualization, Methodology, Software, Formal analysis, Investigation, Validation, Writing – original draft, Writing – review & editing, Supervision. **Stefania Santini:** Conceptualization, Methodology, Software, Formal analysis, Investigation, Validation, Writing – original draft, Writing – review & editing, Supervision.

Declaration of competing interest

The authors declare that they have no known competing financial interests or personal relationships that could have appeared to influence the work reported in this paper.

Data availability

No data was used for the research described in the article.

Acknowledgment

This work has been partially funded by the project KINEBRAIN, CUP:B61B19000430008.

References

Araque, E.S., Colin, G., Cloarec, G.-M., Ketfi-Cherif, A., Chamaillard, Y., 2018. Energy analysis of eco-driving maneuvers on electric vehicles. IFAC-PapersOnLine 51 (31), 195–200.

Basrah, M.S., Siampis, E., Velenis, E., Cao, D., Longo, S., 2017. Wheel slip control with torque blending using linear and nonlinear model predictive control. Veh. Syst. Dyn. 55 (11), 1665–1685.

Bifulco, G.N., Coppola, A., Loizou, S.G., Petrillo, A., Santini, S., 2021. Combined energy-oriented path following and collision avoidance approach for autonomous electric vehicles via nonlinear model predictive control. In: 2021 IEEE International Conference on Environment and Electrical Engineering and 2021 IEEE Industrial and Commercial Power Systems Europe. EEEIC/I&CPS Europe, IEEE, pp. 1–6.

Bifulco, G.N., Coppola, A., Petrillo, A., Santini, S., 2022. Decentralized cooperative crossing at unsignalized intersections via vehicle-to-vehicle communication in mixed traffic flows. J. Intell. Transp. Syst. 1–26. http://dx.doi.org/10.1080/15472450.2022.2124868.

Caiazzo, B., Lui, D.G., Petrillo, A., Santini, S., 2021. Distributed double-layer control for coordination of multiplatoons approaching road restriction in the presence of IoV communication delays. IEEE Internet Things J. 9 (6), 4090–4109.

Cappiello, R., Rosa, F.D., Petrillo, A., Santini, S., 2021. Eco-driving adaptive cruise control via model predictive control enhanced with improved grey wolf optimization algorithm. In: Optimization and Data Science: Trends and Applications. Springer, pp. 139–153.

Chen, G., Hua, M., Zong, C., Zhang, B., Huang, Y., 2019. Comprehensive chassis control strategy of FWIC-EV based on sliding mode control. IET Intell. Transp. Syst. 13 (4), 703–713.

Chen, J., Yu, J., Zhang, K., Ma, Y., 2018. Control of regenerative braking systems for four-wheel-independently-actuated electric vehicles. Mechatronics 50, 394–401.

Chhikara, R., Garg, R., Chhabra, S., Karnatak, U., Agrawal, G., 2021. Factors affecting adoption of electric vehicles in India: An exploratory study. Transp. Res. D Transp. Environ. 100, 103084.

Coppola, A., Lui, D.G., Petrillo, A., Santini, S., 2022. Eco-driving control architecture for platoons of uncertain heterogeneous nonlinear connected autonomous electric vehicles. IEEE Trans. Intell. Transp. Syst. 23 (12), 24220–24234.

Cortés, P., Kouro, S., La Rocca, B., Vargas, R., Rodríguez, J., León, J.I., Vazquez, S., Franquelo, L.G., 2009. Guidelines for weighting factors design in model predictive control of power converters and drives. In: 2009 IEEE International Conference on Industrial Technology. IEEE, pp. 1–7.

De Castro, R., Araújo, R.E., Freitas, D., 2012. Wheel slip control of EVs based on sliding mode technique with conditional integrators. IEEE Trans. Ind. Electron. 60 (8), 3256–3271.

Egbue, O., Long, S., 2012. Barriers to widespread adoption of electric vehicles: An analysis of consumer attitudes and perceptions. Energy Policy 48, 717–729.

Fiori, C., Ahn, K., Rakha, H.A., 2016. Power-based electric vehicle energy consumption model: Model development and validation. Appl. Energy 168, 257–268.

Fiori, C., Marzano, V., Punzo, V., Montanino, M., 2020. Energy consumption modeling in presence of uncertainty. IEEE Trans. Intell. Transp. Syst. 22 (10), 6330–6341.

Gang, L., Zhi, Y., 2018. Energy saving control based on motor efficiency map for electric vehicleswith four-wheel independently driven in-wheel motors. Adv. Mech. Eng. 10 (8), 1687814018793064.

Genta, G., Morello, L., 2019. The Automotive Chassis: Volume 2: System Design. Springer Nature.

Guiggiani, M., 2014. The Science of Vehicle Dynamics. Springer Netherlands, Pisa, Italy, p. 15.

Guo, L., Gao, B., Gao, Y., Chen, H., 2016. Optimal energy management for HEVs in eco-driving applications using bi-level MPC. IEEE Trans. Intell. Transp. Syst. 18 (8), 2153–2162.

Guo, J., Li, W., Wang, J., Luo, Y., Li, K., 2021. Safe and energy-efficient car-following control strategy for intelligent electric vehicles considering regenerative braking. IEEE Trans. Intell. Transp. Syst.

Guo, H., Wang, X., Li, L., 2019. State-of-charge-constraint-based energy management strategy of plug-in hybrid electric vehicle with bus route. Energy Convers. Manage. 199, 111972.

Helton, J.C., Davis, F.J., 2003. Latin hypercube sampling and the propagation of uncertainty in analyses of complex systems. Reliab. Eng. Syst. Saf. 81 (1), 23–69.

Huang, X., Wang, J., 2012. Model predictive regenerative braking control for lightweight electric vehicles with in-wheel motors. Proc. Inst. Mech. Eng. D 226 (9), 1220–1232.

Kanarachos, S., Alirezaei, M., Jansen, S., Maurice, J.-P., 2014. Control allocation for regenerative braking of electric vehicles with an electric motor at the front axle using the state-dependent Riccati equation control technique. Proc. Inst. Mech. Eng. D 228 (2), 129–143.

Ko, J., Ko, S., Kim, I., Hyun, D., Kim, H., 2014a. Co-operative control for regenerative braking and friction braking to increase energy recovery without wheel lock. Int. J. Automot. Technol. 15 (2), 253–262.

Ko, J., Ko, S., Son, H., Yoo, B., Cheon, J., Kim, H., 2014b. Development of brake system and regenerative braking cooperative control algorithm for automatic-transmission-based hybrid electric vehicles. IEEE Trans. Veh. Technol. 64 (2), 431–440.

Kovačić, M., Mutavdžija, M., Buntak, K., 2022. New paradigm of sustainable urban mobility: Electric and autonomous vehicles—A review and bibliometric analysis. Sustainability 14 (15), 9525.

Kumar, C.N., Subramanian, S.C., 2016. Cooperative control of regenerative braking and friction braking for a hybrid electric vehicle. Proc. Inst. Mech. Eng. D 230 (1), 103–116.

Lee, W.J., Kwag, S.I., Ko, Y.D., 2021. The optimal eco-friendly platoon formation strategy for a heterogeneous fleet of vehicles. Transp. Res. D Transp. Environ. 90, 102664.

Li, W., Du, H., Li, W., 2018. Driver intention based coordinate control of regenerative and plugging braking for electric vehicles with in-wheel PMSMs. IET Intell. Transp. Syst. 12 (10), 1300–1311.

Li, L., Ping, X., Shi, J., Wang, X., Wu, X., 2021. Energy recovery strategy for regenerative braking system of intelligent four-wheel independent drive electric vehicles. IET Intell. Transp. Syst.

Li, L., Zhang, Y., Yang, C., Yan, B., Martinez, C.M., 2016. Model predictive control-based efficient energy recovery control strategy for regenerative braking system of hybrid electric bus. Energy Convers. Manage. 111, 299–314.

Liu, J., Wang, Z., Hou, Y., Qu, C., Hong, J., Lin, N., 2021. Data-driven energy management and velocity prediction for four-wheel-independent-driving electric vehicles. ETransportation 9, 100119.

Lv, C., Zhang, J., Li, Y., 2014. Extended-Kalman-filter-based regenerative and friction blended braking control for electric vehicle equipped with axle motor considering damping and elastic properties of electric powertrain. Veh. Syst. Dyn. 52 (11), 1372–1388.

Lv, C., Zhang, J., Li, Y., Yuan, Y., 2015. Mode-switching-based active control of a powertrain system with non-linear backlash and flexibility for an electric vehicle during regenerative deceleration. Proc. Inst. Mech. Eng. D 229 (11), 1429–1442.

Maia, R., Silva, M., Araújo, R., Nunes, U., 2015. Electrical vehicle modeling: A fuzzy logic model for regenerative braking. Expert Syst. Appl. 42 (22), 8504–8519.

Manfredi, S., Petrillo, A., Santini, S., 2020. Distributed PI control for heterogeneous nonlinear platoon of autonomous connected vehicles. IFAC-PapersOnLine 53 (2), 15229–15234.

Maybury, L., Corcoran, P., Cipcigan, L., 2022. Mathematical modelling of electric vehicle adoption: A systematic literature review. Transp. Res. D Transp. Environ. 107, 103278.

Mruzek, M., Gajdáč, I., Kučera, L., Gajdošík, T., 2017. The possibilities of increasing the electric vehicle range. Procedia Eng. 192, 621–625.

Nam, K., Fujimoto, H., Hori, Y., 2012. Lateral stability control of in-wheel-motor-driven electric vehicles based on sideslip angle estimation using lateral tire force sensors. IEEE Trans. Veh. Technol. 61 (5), 1972–1985.

Nian, X., Peng, F., Zhang, H., 2014. Regenerative braking system of electric vehicle driven by brushless DC motor. IEEE Trans. Ind. Electron. 61 (10), 5798–5808.

Onat, N.C., Kucukvar, M., 2022. A systematic review on sustainability assessment of electric vehicles: Knowledge gaps and future perspectives. Environ. Impact Assess. Rev. 97, 106867.

Pacejka, H., 2005. Tire and Vehicle Dynamics. Elsevier.

Pariota, L., Coppola, A., Di Costanzo, L., Di Vico, A., Andolfi, A., D'Aniello, C., Bifulco, G.N., 2020. Integrating tools for an effective testing of connected and automated vehicles technologies. IET Intell. Transp. Syst. 14 (9), 1025–1033.

Petrillo, A., Prati, M.V., Santini, S., Tufano, F., 2023. Improving the NOx reduction performance of an Euro VI d SCR System in real-world condition via nonlinear model predictive control. Int. J. Engine Res. 24 (3), 823–842.

Rajamani, R., 2011. Vehicle Dynamics and Control. Springer Science & Business Media.

Ruan, J., Walker, P.D., Watterson, P.A., Zhang, N., 2016. The dynamic performance and economic benefit of a blended braking system in a multi-speed battery electric vehicle. Appl. Energy 183, 1240–1258.

Sun, D.J., Zheng, Y., Duan, R., 2021. Energy consumption simulation and economic benefit analysis for urban electric commercial-vehicles. Transp. Res. D Transp. Environ. 101, 103083.

Tao, Y., Xie, X., Zhao, H., Xu, W., Chen, H., 2017. A regenerative braking system for electric vehicle with four in-wheel motors based on fuzzy control. In: 2017 36th Chinese Control Conference. CCC, IEEE, pp. 4288–4293.

Tzirakis, E., Pitsas, K., Zannikos, F., Stournas, S., 2006. Vehicle emissions and driving cycles: comparison of the Athens driving cycle (ADC) with ECE-15 and European driving cycle (EDC). Glob. NEST J. 8 (3), 282–290.

Valentina, A., Maria, A.R., Carmelo, A., Davide, A., Ricardo, R.B., Filipe, B.E.S., Peter, B., Paolo, B., Flavio, B., Ioris, B., et al., 2019. The Future of Cities: Opportunities, Challenges and the Way Forward. Technical Report, Joint Research Centre (Seville site).

Wang, B., Huang, X., Wang, J., Guo, X., Zhu, X., 2015. A robust wheel slip ratio control design combining hydraulic and regenerative braking systems for in-wheel-motors-driven electric vehicles. J. Franklin Inst. B 352 (2), 577–602.

Wang, Y., Wang, X., Sun, Y., You, S., 2018. Model predictive control strategy for energy optimization of series-parallel hybrid electric vehicle. J. Clean. Prod. 199, 348–358.

Wu, Y.-C., Kontou, E., 2022. Designing electric vehicle incentives to meet emission reduction targets. Transp. Res. D Transp. Environ. 107, 103320.

Wu, Y., Li, S.E., Cortés, J., Poolla, K., 2019. Distributed sliding mode control for nonlinear heterogeneous platoon systems with positive definite topologies. IEEE Trans. Control Syst. Technol.

Xiao, B., Lu, H., Wang, H., Ruan, J., Zhang, N., 2017. Enhanced regenerative braking strategies for electric vehicles: Dynamic performance and potential analysis. Energies 10 (11), 1875.

Xin, Y., Zhang, T., Zhang, H., Zhao, Q., Zheng, J., Wang, C., 2019. Fuzzy logic optimization of composite brake control strategy for load-isolated electric bus. Math. Probl. Eng. 2019.

Xu, W., Chen, H., Zhao, H., Ren, B., 2019. Torque optimization control for electric vehicles with four in-wheel motors equipped with regenerative braking system. Mechatronics 57, 95–108.

Xu, G., Xu, K., Zheng, C., Zhang, X., Zahid, T., 2015. Fully electrified regenerative braking control for deep energy recovery and maintaining safety of electric vehicles. IEEE Trans. Veh. Technol. 65 (3), 1186–1198.

Zhang, X., Göhlich, D., Li, J., 2017. Energy-efficient toque allocation design of traction and regenerative braking for distributed drive electric vehicles. IEEE Trans. Veh. Technol. 67 (1), 285–295.

Zhang, J., Lv, C., Gou, J., Kong, D., 2012. Cooperative control of regenerative braking and hydraulic braking of an electrified passenger car. Proc. Inst. Mech. Eng. D 226 (10), 1289–1302.

Zhang, J., Lv, C., Qiu, M., Li, Y., Sun, D., 2013. Braking energy regeneration control of a fuel cell hybrid electric bus. Energy Convers. Manage. 76, 1117–1124.

Zhao, D., Chu, L., Xu, N., Sun, C., Xu, Y., 2018. Development of a cooperative braking system for front-wheel drive electric vehicles. Energies 11 (2), 378.